Stephanie Moyerman
MA 164
Final Project
04/28/2006

Exploring the Lorenz Equations through a Chaotic Waterwheel

# 1 Introduction

The Lorenz equations

$$\dot{x} = \sigma(y - x) \tag{1a}$$
$$\dot{y} = rx - y - xz \tag{1b}$$
$$\dot{z} = xy - bz \tag{1c}$$

were derived by Edward Lorenz in 1963 as an over-simplified model of convection rolls within the atmosphere [1]. These coupled differential equations appear quite harmless; only two terms appear that cause non-linearity. Lorenz found, however, that the behavior of the system changed drastically over a wide range of parameters. For certain parameter values, Lorenz discovered that the system exhibited unpredictable and even chaotic behavior!

Our goal in this paper is to directly explore the properties of the Lorenz equations and their exact mechanical analog, a chaotic waterwheel. In subsequent sections, the reader will encounter the derivation of these amazing equations, an exploration of parameter space, computational results and trajectories, and an in-depth look at chaos.

# 2 Derivation

We will derive the Lorenz equations by first deriving the equations of motion for a chaotic waterwheel and then performing a change of variables.

A schematic diagram of a chaotic waterwheel is given in Figure 1 on the next page. The wheel rests atop a flat surface and is tilted slightly from the horizontal. Water is pumped into the system through a perforated hose at the top and directed into dozens of small nozzles. The nozzles distribute the water at a steady rate into chambers around the side of the wheel. A small hole at the bottom of each chamber allows water to leak out, resulting in a time dependent volume of water in each chamber.

Let us now define our variables and parameters and explain what each entails:

- $\theta$ := the angle of rotation in the lab frame
- $\omega(t)$ := angular velocity of the wheel, increasing in the counterclockwise direction

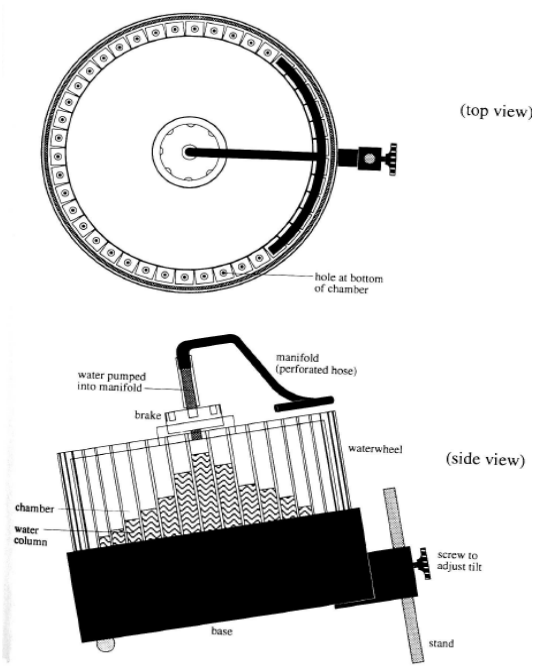


Figure 1: Illustration of the chaotic waterwheel [2]

- $m(\theta, t)$:= mass distribution of water around the rim of the wheel. The total mass of water between any two points, $\theta_1$ and $\theta_2$ is given by

$$M(t) := \int_{\theta_1}^{\theta_2} m(\theta, t) d\theta$$

- $Q(\theta)$ := rate at which water is pumped into the chambers
- $r$ := radius of the wheel
- $g$ := gravity, which can be changed by increasing or decreasing the tilt of the waterwheel
- $\nu$ := rotational damping rate, which can be altered by increasing or decreasing the friction in the brake
- $I$ := moment of inertia of the wheel

Our goal is to derive equations governing $\omega(t)$ and $m(\theta, t)$ and then convert these equations into a system of ODEs. To do so, we use conservation of mass, torque balance, the amplitude equations, and a little bit of magic.

## 2.1 Conservation of Mass

Consider any section of the waterwheel from $\theta_1$ to $\theta_2$. Within any such section, there are four contributions that govern how the mass changes in a time $\Delta t$:

1. Total mass of inflow water from the pump, given by $\Big[\int_{\theta_1}^{\theta_2} Q d\theta\Big]$.

2. The mass of water that leaks from the system, $\Big[-\int_{\theta_1}^{\theta_2} K m d\theta\Big]\Delta t$. The factor of $m$ in the integral is very important. It means that the rate at which water flows out of a region is proportional to the mass contained within, which matches experimental data [2]. It also ensures that water will never flow from a region with no mass enclosed.

3. The mass carried in by the rotating wheel. This is given by $m\theta_1\omega\Delta t$, where $m\theta_1$ is the mass per unit angle and $\omega\Delta t$ is the angular width.

4. Similarly, the mass that rotates out is $-m\theta_2\omega\Delta t$.

Combining these yields

$$\delta M = \Delta t\Big[\int_{\theta_1}^{\theta_2} Q d\theta - \int_{\theta_1}^{\theta_2} K m d\theta\Big] + m\theta_1\omega\Delta t - m\theta_2\omega\Delta t.$$

Pulling the rotational terms into the integral, dividing by $\Delta t$ and taking the limit as $\Delta t \to 0$ gives

$$\frac{dM}{dt} = \int_{\theta_1}^{\theta_2} (Q - Km - \omega\frac{\partial m}{\partial \theta}) d\theta.$$

Now, exploiting the definition of mass

$$\frac{dM}{dt} = \int_{\theta_1}^{\theta_2} \frac{\partial m}{\partial t} d\theta,$$

we have

$$\int_{\theta_1}^{\theta_2} \frac{\partial m}{\partial t} d\theta = \int_{\theta_1}^{\theta_2} (Q - Km - \omega\frac{\partial m}{\partial \theta}) d\theta.$$

As this must hold over any arbitrary interval, the integrands must be equal. This gives what is known as our continuity equation:

$$\frac{\partial m}{\partial t} = Q - Km - \omega\frac{\partial m}{\partial \theta}. \tag{2}$$

## 2.2 Torque Balance

To derive our governing equation for $\omega$, we consider the torques applied to the waterwheel. We first note that as $t \to \infty$, the moment of inertia, $I$, of the wheel tends to a constant value [2]. Thus we will treat the moment of inertia as a constant in our derivation. This leaves two sources of torque, damping and gravity.

There are two sources of rotational damping in the waterwheel. The first is the brake, which can be adjusted by the user. The second is the introduction of water with $\omega_0 = 0$,

which must gain momentum until it reaches the system's velocity $\omega_f = \omega$. As both of factors are proportional to the angular velocity, we represent this torque as

$$\text{damping torque} = -\nu\omega,$$

where $\nu > 0$.

Finally, for an infinitesimal angle $d\theta$, there is a gravitational torque on the system given by

$$d\tau = mgr \sin\theta d\theta.$$

Here, $g = g_0 \sin\alpha$, is the effective gravity, which depends upon the tilt of the waterwheel from horizontal, $\alpha$. Integrating over the total mass and combining with the damping torque yields

$$\tau = I\dot{\omega} = -\nu\omega + gr\int_0^{2\pi} m(\theta, t)\sin\theta d\theta, \tag{3}$$

the equation governing our angular velocity.

## 2.3 Amplitude Equations

Equations (2) and (3) appear to be a set of very complicated partial, coupled differential equations. We will now apply the amplitude equations and see the magic happen.

Since the mass is $2\pi$ periodic in $\theta$, we may rewrite it as a Fourier series

$$m(\theta, t) = \sum_{n=0}^{\infty} [a_n(t)\sin n\theta + b_n(t)\cos n\theta],$$

where substitution into equations (2) and (3) will yield differential equations for $a_n$ and $b_n$, known as amplitude equations. We may also write the inflow as a Fourier series

$$Q(\theta) = \sum_{n=0}^{\infty} q_n \cos n\theta,$$

where the sin term is neglected since the inflow is assumed to be symmetric about $\theta = 0$ (the top of the waterwheel).

Substituting our series representations for $m$ and $Q$ into (2) and collecting $\sin n\theta$ and $\cos n\theta$ terms gives

$$\dot{a_n} = n\omega b_n - Ka_n\dot{b_n} = -n\omega a_n - Kb_n + q_n. \tag{4}$$

We may now recast our equation governing $\omega$ in terms of Fourier series as

$$\begin{aligned} I\dot{\omega} &= -\nu\omega + gr\int_0^{2\pi}\Big[\sum_{n=0}^{\infty} a_n(t)\sin n\theta + b_n(t)\cos n\theta\Big]\sin\theta d\theta \\ &= -\nu\omega + gr\int_0^{2\pi} a_1 \sin^2\theta d\theta \\ &= -\nu\omega + \pi gr a_1, \end{aligned}$$

where all the other terms have integrated to zero by orthogonality. Thus $a_1$, $b_1$, and $\omega$ form a closed system, decoupled from all higher order modes. In fact, for all higher modes, $a_n, b_n \to 0$ as $t \to \infty$. The governing equations for our waterwheel are then

$$\dot{a_1} = n\omega b_1 - Ka_1 \tag{5a}$$

$$\dot{b_1} = -n\omega a_1 - Kb_1 + q_1 \tag{5b}$$

$$\dot{\omega} = (-\nu\omega + \pi g r a_1)/I. \tag{5c}$$

### 2.4 Change of Variables: The Lorenz Equations

Our three dimensional waterwheel system is equivalent to the Lorenz system introduced in equation (1). The change of variables is as follows:

$$a_1 = \frac{K\nu}{\pi g r} y$$

$$b_1 = \frac{-K\nu}{\pi g r} z + \frac{q_1}{K}$$

$$\omega = Kx$$

$$t = \frac{\tau}{K},$$

where the Prandtl number is $\sigma = \frac{\nu}{KI}$ and the Rayleigh number is $r = \frac{\pi g r q_1}{K^2 \nu}$. However, note that with this change of variables, the Lorenz equations parameter $b$ (a parameter that actually remains nameless) must be set as $b = 1$, meaning the waterwheel is a specific case of the broader Lorenz equations. Nonetheless, this simple mechanical system has been transformed into one of the most widely studies chaotic systems known today!

## 3 Preliminary Analysis of Systems

### 3.1 The Waterwheel

We begin by exploring the fixed points of equation (5), which are given by:

$$(a_1*, b_1*, w*) = (0, \frac{q_1}{K}, 0)$$

$$(a_1*, b_1*, w*) = (\frac{\nu\omega*}{\pi g r}, \frac{K\nu}{\pi g r}, \pm\frac{\pi g r q_1}{\nu} - K^2),$$

where we have left our value of $\omega*$ in the expression for $a_1*$ for notational convenience.

The first fixed point corresponds to a stationary state. At this fixed point the wheel is not rotating; inflow is balanced exactly by leakage.

The second fixed point corresponds to steady state rotation of the waterwheel in either direction, dependent upon the sign of $\omega$. Such a solution can exist if and only if

$$\frac{\pi g r q_1}{K^2 \nu} > 1,$$

which one might recognize as the Rayliegh number introduced during our change of variables! The Rayleigh number can be thought of as a description of the system's drive versus dissipation. The numerator terms $g$ and $q_1$ tend to spin the wheel, while the denominator terms $K$ and $\nu$ tend to oppose the wheel's motion.

For much larger Rayleigh numbers, the waterwheel begins to exhibit chaotic behavior, analogous to the results we will find for the Lorenz equations. However, the analogy breaks down at even higher Rayleigh numbers, where the waterwheel settles into pendulum-like motion, rotating once counterclockwise, then clockwise, then counterclockwise, etc. No similar steady-state is found for high Rayleigh numbers in the Lorenz equations.

In section 3, we will explore the behavior of the chaotic waterwheel in all three regimes using numerical integration techniques.

## 3.2 The Lorenz Equations

The first thing to note about the Lorenz equations is that they possess a great deal of symmetry. For instance, if we replace any pair $(x, y)$ with $(-x, -y)$, equation (1) is completely unaffected. This fact allows us to cut our analysis in half; any results that we find may immediately be applied to their reflexive partner!

Further, all trajectories of the Lorenz equations are eventually confined to paths of zero volume. To show this, we consider the Lorenz system as a generic function $\dot{\vec{x}} = \vec{f}(\vec{x})$. Then we know from multivariable calculus that

$$\dot{V} = \int_V \nabla \cdot \vec{f} dV, \tag{6}$$

where $V$ is our volume. Taking the divergence of the Lorenz equations gives

$$\begin{aligned} \nabla \cdot \vec{f} &= \frac{\partial}{\partial x}[\sigma(y-x)] + \frac{\partial}{\partial y}[rx - y - xz] + \frac{\partial}{\partial z}[xy - bz] \\ &= -(\sigma + 1 + b) < 0. \end{aligned}$$

As this result is a constant, equation (6) reduces to $\dot{V} = -(\sigma + 1 + b)V$, which has the solution $V(t) = V(0)e^{-(\sigma+1+b)t}$. Thus all trajectories are confined to zero volume exponentially fast! This result imposes many constraints on possible solutions to the Lorenz equations. For instance, quasiperiodic orbits, repelling fixed points, and repelling orbits may all be immediately ruled out.

Now we wish to find and explore the fixed points of equation 1. It is clear that the origin is a fixed point for all values of $\sigma$, $r$, and $b$. We classify it's stability by first noting that the linear expression for $\dot{z}$, found by ommitting the nonlinear $xy$ term, is

$$\dot{z} = -bz.$$

From this equation we see that $z$ is decoupled and that all trajectories decrease to $z = 0$ at an exponential rate. The remaining two equations (neglecting the nonlinear terms) may

be written as

$$\begin{pmatrix} \dot{x} \\ \dot{y} \end{pmatrix} = \begin{bmatrix} -\sigma & \sigma \\ r & -1 \end{bmatrix} \begin{pmatrix} x \\ y \end{pmatrix},$$

where the trace is always $< 0$ and the determinant is given by $\Delta = \sigma(1 - r)$. Thus, for $r < 1$, we have $\Delta > 0$ and the origin is an attracting fixed point. In fact, for $r < 1$, *every* trajectory of the system approaches the origin as $t \to \infty$.

For $r > 1$ the origin becomes a saddle node fixed point. However, two new fixed points emerge

$$C_{\pm} = (\pm\sqrt{b(r-1)}, \pm\sqrt{b(r-1)}, r-1)$$

which are only defined for $r > 1$. These fixed points are linearly stable in the regime

$$a < r < r_h = \frac{\sigma(\sigma + b + 3)}{\sigma - b - 1}$$

as long as $\sigma - b - 1 > 0$ (The stability analysis is omitted here. For a detailed analysis, see [3]). Above $r_h$, the limit cycles of these two fixed points become unstable. What, then, is the behavior of the system at $r > r_h$? Our system has no fixed or periodic points, but certainly all trajectories cannot tend to infinity, as this would violate our volume contraction.

Lorenz used numerical integration techniques to explore this range of parameters. He found that all orbits in this range were eventually confined to a set resembling a pair of infinitely thin, three-dimensional butterfly wings. Further, Lorenz found that the trajectories seemed to move about randomly along this "strange attractor", indicating a chaotic system. This confining set was later named the "Lorenz Attractor", and was found to have fractal dimension, infinite area, and zero volume. A bifurcation diagram illustrating all three behaviors of the system is given below.

There are two defining features of a chaotic system: aperiodic long term behavior and sensitive dependence on initial conditions. Aperiodic long term behavior simply means that trajectories exist that never settle to a fixed point, periodic orbits, or quasiperiodic orbits. Sensitive dependence on initial conditions means that the trajectories of nearby initial conditions diverge exponentially fast.

Through numerical schemes, we will illustrate both of these phenomenon. Aperiodic long term behavior will be shown by direct integration of the Lorenz equations. Sensitive dependence on initial conditions will be shown by calculating the Lyapunov function and comparing the outputs of several solvers for both $r < r_h$ and $r > r_h$. We will also show the divergence of 10,000 nearby initial conditions and generate "fractal" patterns resultant from the waterwheel trajectories in the chaotic regime.

# 4 Goals and Numerics

All numerical simulations were run using Matlab 7.0.4. The following is a brief description of each one.

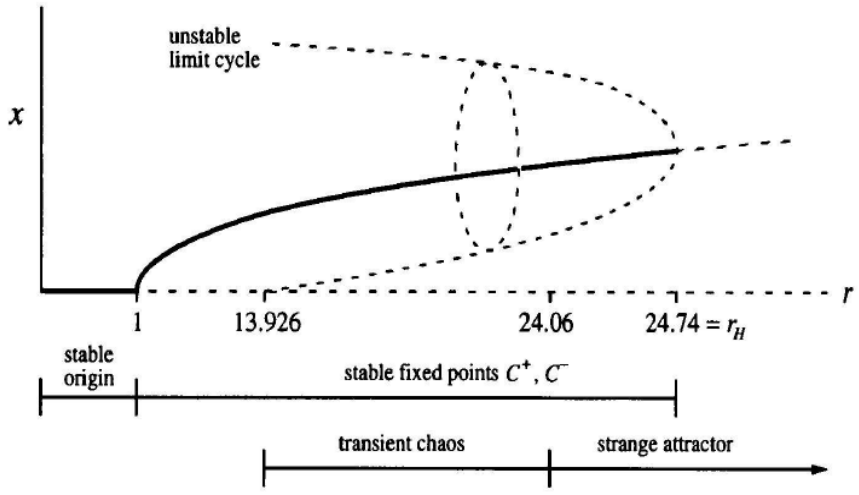


Figure 2: Bifurcation diagram for the Lorenz system. The values of $r$ for which the behavior changes are indicated.

## 4.1 Computing Trajectories: Lorenz Equations and Waterwheel

Direct integration of the Lorenz and waterwheel equations were done using ODE45, which uses an explicit (4,5) Runge-Kutta method for our coupled differential equations. For the Lorenz equations, trajectories of an initial condition and its reflexive partner were calculated for each of the system's behaviors. The waterwheel equations were integrated using a fixed time step (as opposed to the adaptive time step used for the Lorenz equations) and the results for $\theta$ vs $t$ were displayed as a plot and an animation of a point rotating along a wheel.

## 4.2 Lyapunov

The Lyapunov function was found using ODE45 with an adaptive time step. The program chooses a fixed number of random initial conditions (typically 10, with random numbers chosen from the interval (0,1) in each variable) and pairs each with a second nearby initial condition differing in the fourth decimal place. The average difference between the end points of all the pairs is computed at evenly spaced intervals in the range 100–10000 seconds. The results, average distance vs $\log t$, were then plotted.

## 4.3 Comparison of Solvers

A comparison between the ODE45, ODE23, and ODE113 solvers was carried out in the chaotic regime. ODE23 uses a explicit (2,3) Runge-Kutta numerical integration scheme, and is typically less reliable than ODE45 when accurate precision is required. ODE113 is a variable Adams-Bachforth-Moulton PECE solver, which is more efficient than ODE45 when solving problems with small tolerances and problems that are very computationally expensive.

The code itself creates an array of $N$ random starting points (typically 10 points with random numbers chosen from the interval (0,1) using a normal distribution), and evaluates the average final position of these points for each solver at times from 0–60 s in increments of 1 second. The results of each solver are plotted vs time for comparison.

### 4.4 Divergence of Trajectories

This program uses ODE45 to solve for the end points of 10,000 nearby (varying in the fourth decimal place) trajectories. All initial conditions begin close to the origin, and their final positions at a specified time $t$ are plotted on top of the Lorenz Butterfly for comparison.

### 4.5 Fractal Patterns

Fractal patterns (which are techinically not fractals because they possess no inherent self similarity) were generated in two ways. In each of the following methods, ODE45 was used to compute the trajectories of 90,000 initial conditions, producing a 300x300 grid solution.

1. Sensitive dependence on initial conditions was shown by numerically integrating the Lorenz equations for a fixed time $t$ at 90,000 initial conditions on a specified window. If the final position of the trajectory was on the right hand side of the butterfly, i.e.– $x > 0$, then a point was plotted in red at the corresponding initial condition. If the final location was on the left hand side, the point was plotted in blue. All computations were done assuming the initial condition $z_0 = 5$ which was chosen arbitrarily. For computational efficiency, ODE45 was set as a fixed interval integrator, where the interval was varied depending on the final time.

2. Patterns were also generated by finding the side of the butterfly on which each trajectory spent more time. As stated above, ODE45 was used to integrate 90,000 initial conditions with $z_0 = 5$ in a specified window for a specified length of time. Again, the integrator was set to perform calculations at fixed time intervals. The solution array was then checked to see if more time was spent where $x < 0$ or $x > 0$. For $x > 0$ a point was plotted in red, and for $x < 0$ a point was plotted in blue.

## 5 Results

### 5.1 The Waterwheel

The results of the waterwheel simulation can be seen below for the steady rotation regime.

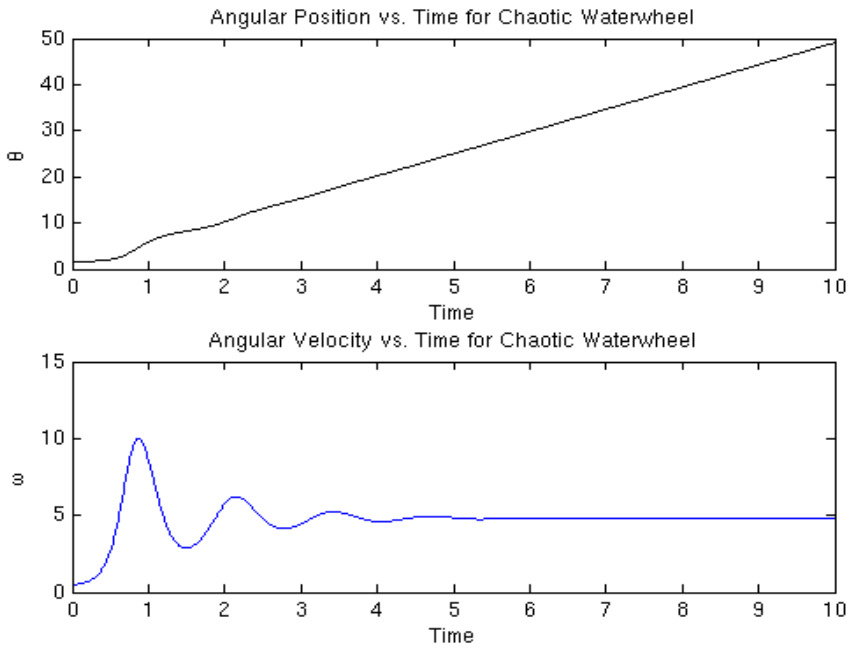


Figure 3: Theta vs. t and Omega vs. t plots corresponding to steady rotation of the waterwheel.

The parameters for this plot are

$$\begin{aligned} K &= 10 \\ q_1 &= 50 \\ \nu &= 0.25 \\ g &= 6 \\ r &= 0.35 \\ I &= 1. \end{aligned}$$

There are several things to note from this figure. First, for $t < 5$, the waterwheel has large spikes in angular velocity. As the waterwheel spins, braking and friction slow the system to a state of no rotation. However, this state is unstable, and as water pours into the system the wheel quickly begins rotating. This is the spike we observe in the velocity. However, for times relatively close to zero the waterwheel does not have enough inertia to keep spinning, i.e.- braking and friction win again. This process repeats until the waterwheel has enough inertia (contains enough water) to spin perpetually on a sudden burst. In our plot, this occurs at roughly $t = 6$ s. The plot of angular position vs. time shows a linear increase in $\theta$, and angular velocity vs. time has become a flat line.

One frame of the corresponding animations is plotted in Figure 4 below. The red circle indicates the position of the initial condition at time $t$. As the dot rotates, we form a picture of the waterwheel's motion.

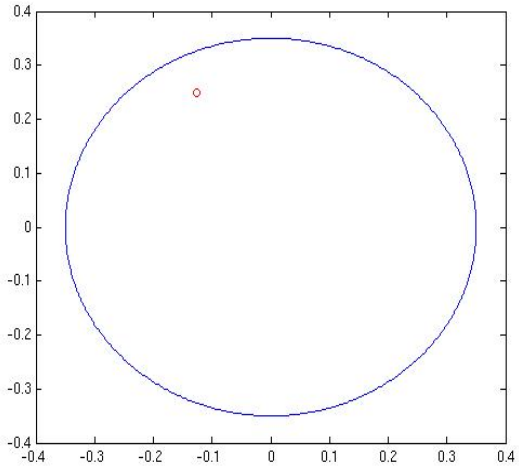


Figure 4: Theta vs. t and Omega vs. t plots corresponding to steady rotation of the waterwheel.

## 5.2 The Lorenz Equations

Figure 5 shows four possible behaviors of the chaotic waterwheel: stable origin, stable attractors, transient chaos, and chaos. A picture of the Lorenz butterfly is given in Figure 4(d). One can easily see from these images how the behavior of the system becomes more chaotic as $r$ is increased. Note that $\sigma = 10$ and $b = 2.5$ are constant throughout. The trajectory drawn in red corresponds to the initial condition $[1, 1, 1]$ whereas the trajectory drawn in blue corresponds to $[-1, -1, -1]$. Note the symmetry of these trajectories.

The comparison of solvers is shown in Figure 6. For short time periods the solvers are convergent upon the same solutions in all three coordinates, after which time the solvers quickly diverge. The parameters for these plots are $r = 28$, $\sigma = 10$, and $b = 2.5$.

Figure 7 shows the average value of the magnitude of the solution at time 60 s, with $r = 28$ and $r = 50$ ($\sigma = 10$ and $b = 2.5$). Note that the magnitude plots diverge immediately, but the difference between the solvers does not blow up with time. The divergence seems to be random, varying between 0 and 10 in absolute difference. ODE23 also appears to have very sharp spikes in magnitude while the others do not. Perhaps this is due to ODE23 having the greatest associated error in integration. The solvers appear to have the same differences in magnitude for $r = 28$, at the onset of chaos, and $r = 50$, well into the chaotic regime.

The Lyapunov exponent was calculated in the stable and chaotic regime. Figure 8 (a) shows the Lyapunov calculation for $r = 10$. Notice that the nearby trajectories are immediately drawn to essentially 0 difference. The trajectories converge exponentially with time. However, in Figure 8 (b) we see that the trajectories diverge exponentially with time. By $t = 10$ s the trajectories have diverged by approximately 3x their initial magnitude.

Figure 9 displays the endpoints of 10,000 nearby trajectories at times $t = 0, 1, 20$ and 30 s. The endpoints are plotted in red atop the Lorenz Butterfly which has been plotted

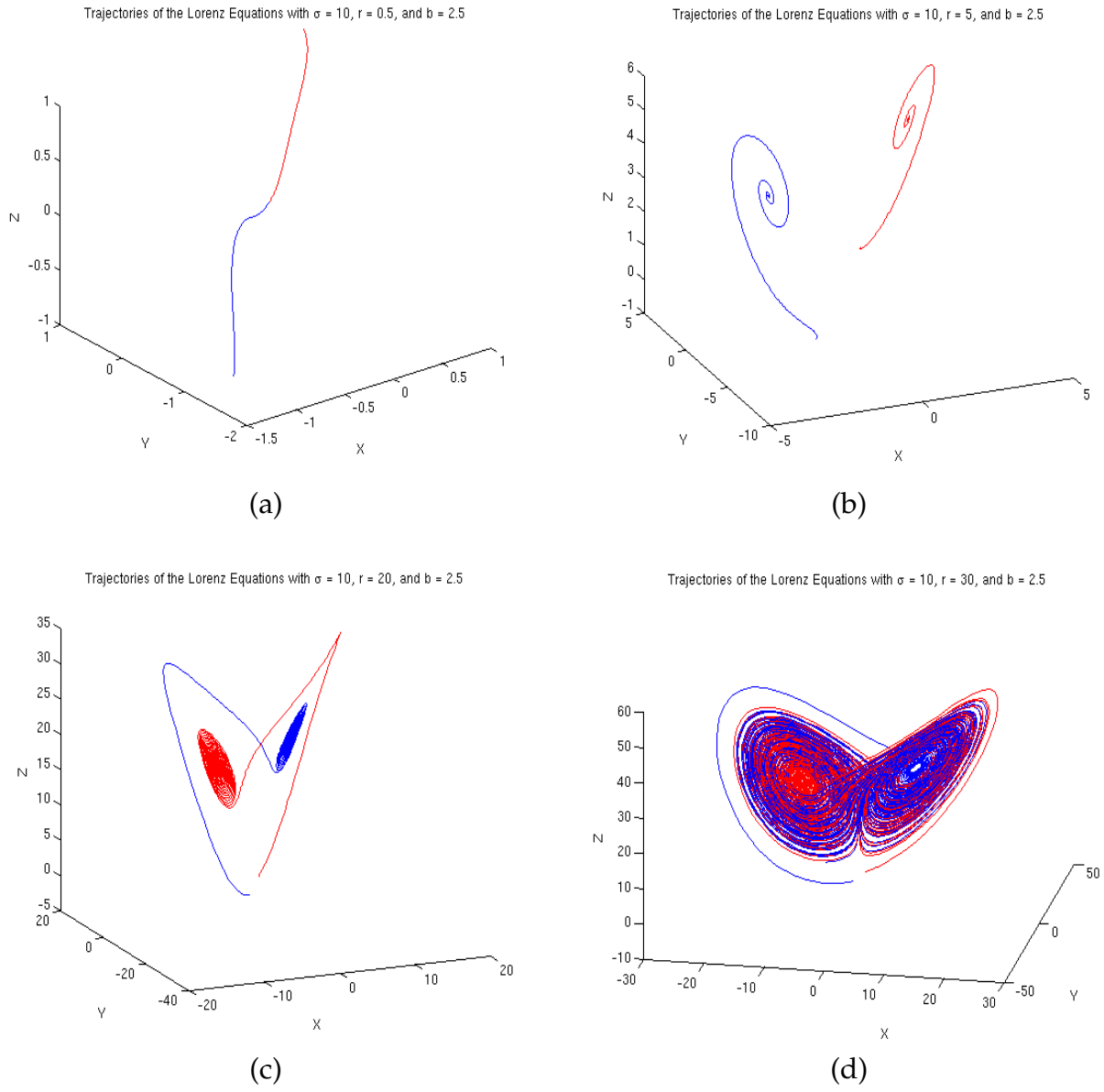


Figure 5: Trajectories of the Lorenz equations showing all four behaviors of the system: (a) the stable origin, (b) two stable attractors, (c) transient chaos, and (d) chaos.

in blue. At $t = 0$ we see the intial positions of all the trajectories. At $t = 1$ we notice that the trajectories have already become quite divergent. At $t = 20$ and $t = 30$ notice that the endpoints no longer form a pattern, but are dispersed in a seemingly random pattern covering the Lorenz Butterfly.

The fractal patterns are, for lack of a better term, completely sweet. Figure 10 below displays the fractal patterns generated by the sensitive dependence on initial conditions. The window used for all 3 plots is $x = [-5, 5]$ and $y = [-5, 5]$. Figure 10(a) shows the final position of trajectories after $t = 1$ seconds. It is clear from this picture that trajectories that are ininitially close can be found on the same half of the butterfly after only one

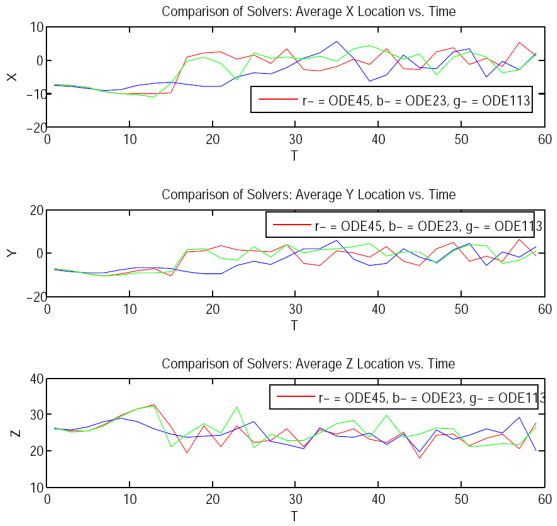


Figure 6: A comparison of ODE45 (red), ODE23 (blue), and ODE113 (green).

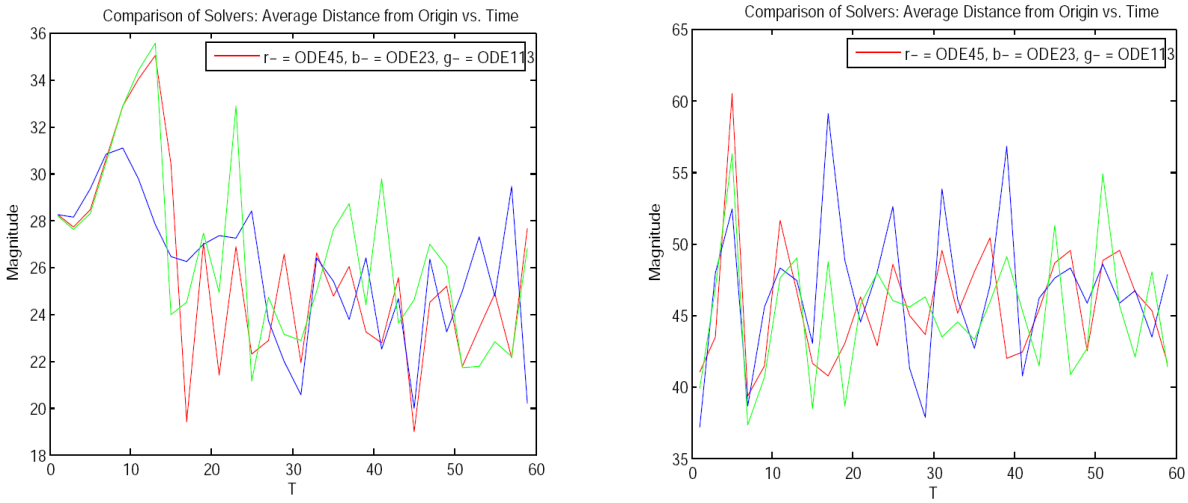


(a) (b)

Figure 7: A comparison of magnitudes for ODE45 (red), ODE23 (blue), and ODE113 (green) at times (a) t=28 s and (b) t=60 s.

second. Figure 10(b) shows a more complicated structure at $t = 5$ s. We see that the trajectories are beginning to diverge based on their sensitive dependence, but an overall structure can still be seen. A blow up of the region $x = [0, 4]$ and $y = [-4, 0]$ (Figure 11) shows that regions that appear all the same color have no deeper hidden structure hiddin within. Figure 10(c), the endpoints of trajectories after $t = 20$ s, shows an extreme sensitive dependence on initial conditions. The final positions have become extremely scattered; it can easily be seen that nearby trajectories end at points on opposite sides of the butterfly. We also note that there is a great deal of symmetry within these plots, as predicted by the original equations. The relevant parameters for these plots are $\sigma = 10$,

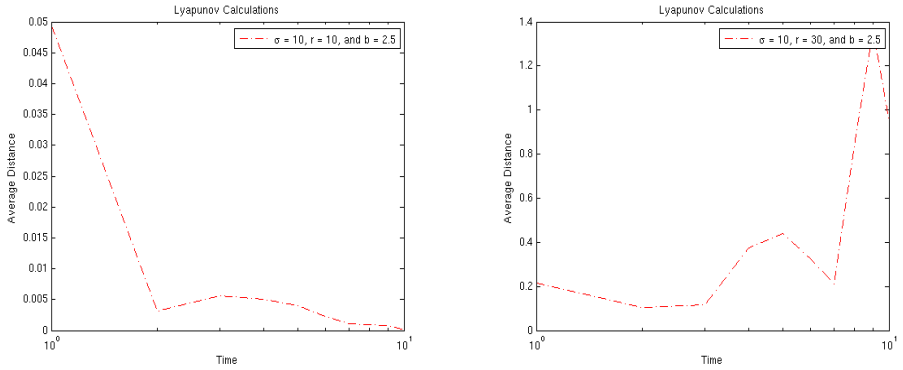


(a) (b)

Figure 8: Plot of calculating the Lyapunov exponent of the system.

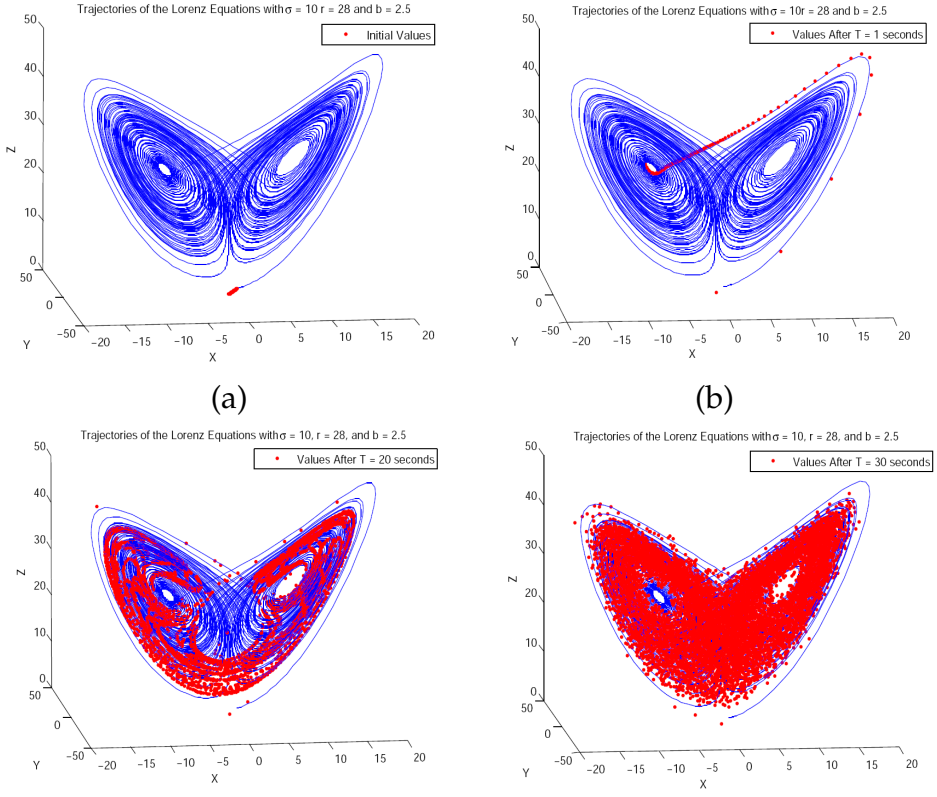


(a) (b)

(c) (d)

Figure 9: The divergence of the endpoints for 10,000 nearby initial conditions.

$r = 40$, and $b = 10$.

Finally, Figure 12 shows the results of the time analysis of the system's trajectories. Remember that if the trajectory of an initial condition spends the majority of its time in the right half of the butterfly it is colored red, else it is colored blue. Figure 12(a) shows results after 5 seconds, which look identical to Figure 11(a). It appears that the location of the trajectory after $t = 1$ seconds dictates where the majority of the time has been spent

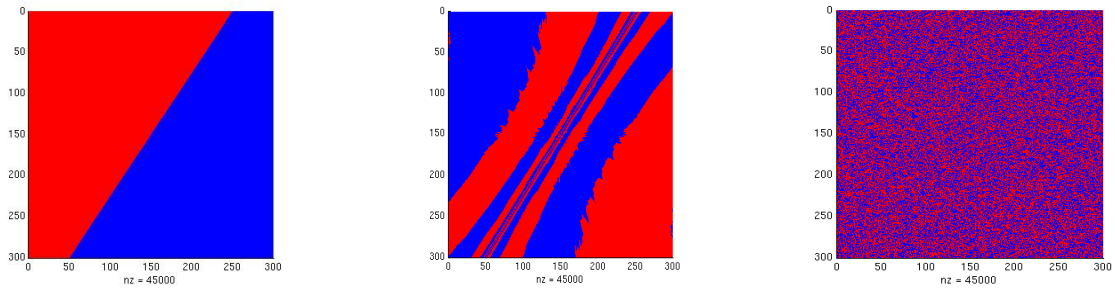


(a) (b) (c)

Figure 10: Fractal patterns generated using the endpoints of trajectories for the Lorenz equations at (a) t=1 s, (b) t=5 s, and (c) t=20 s.

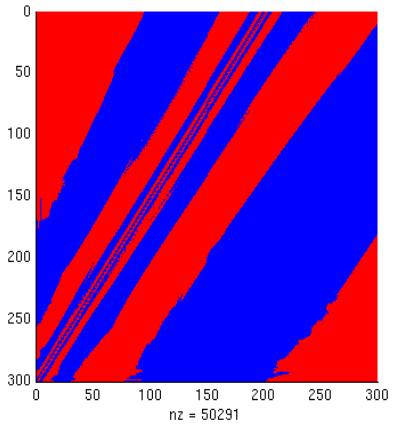


Figure 11: A blow up of Figure 9(c) with $y = [-4, 0]$ and $x = [0, 4]$.

after five seconds time. After $t = 10$ seconds, we see that the line of symmetry has become blurred, and that, in a structured way, a number of points that had spent more time in one half of the butterfly (after $t = 5$ seconds) have now switched. The plot for $t = 20$ (Figure 12(c)) has the same overall structure as $t = 10$ s, but has an increased complexity, which we expect as we iterate further in time in this chaotic regime. Again, in all three pictures, we see symmetry along the same axis as displayed in Figure 11. For all plots displayed, the windows were $x = [-5, 5]$ and $y = [-5, 5]$ and the parameters were $\sigma = 10$, $r = 40$, and $b = 2.5$.

# 6 Conclusions

I have performed an in-depth analysis of the chaotic waterwheel and the Lorenz equations, starting from the derivation of equations and analytical results and working up towards computational findings based on solvers and sensitive dependence on initial conditions. I was able to explore the beautiful inner workings of chaos, generating "fractal" images of increasing complexity.

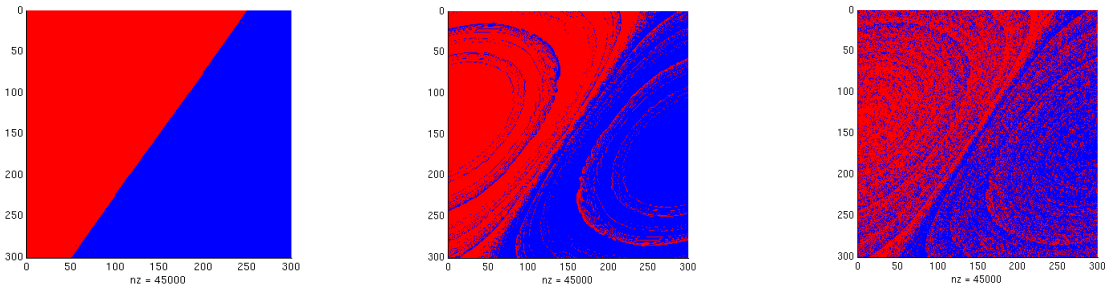


(a) (b) (c)

Figure 12: Fractal patterns generated by analyzing the majority of time spent by trajectories at (a) t=5 s, (b) t=10 s, and (c) t=20 s.

# 7 Works Cited

[1] Lorenz, E. *Deterministic Nonperiodic Flow.* Journal of Atmospheric Sciences, 1963.

[2] Strogatz S.H. *Nonlinear Dynamics and Chaos: With Applications to Physics, Biology, Chemistry, and E* Reading, MA: Perseus Books, Cambridge MA, 1994.

[3] Marsden and McCracken, Springer-Verlag, 327-353, 1976.